Observational hertzsprung-russell diagrams

A&A 616, A10 (2018)
https://doi.org/10.1051/0004-6361/201832843

Astronomy & Astrophysics

Special issue

Gaia Data Release 2

Gaia Data Release 2

Observational Hertzsprung-Russell diagrams★

Gaia Collaboration, C. Babusiaux[1,2,★★], F. van Leeuwen[3], M. A. Barstow[4], C. Jordi[5], A. Vallenari[6], D. Bossini[6], A. Bressan[7], T. Cantat-Gaudin[6,5], M. van Leeuwen[3], A. G. A. Brown[8], T. Prusti[9], J. H. J. de Bruijne[9], C. A. L. Bailer-Jones[10], M. Biermann[11], D. W. Evans[3], L. Eyer[12], F. Jansen[13], S. A. Klioner[14], U. Lammers[15], L. Lindegren[16], X. Luri[5], F. Mignard[17], C. Panem[18], D. Pourbaix[19,20], S. Randich[21], P. Sartoretti[2], H. I. Siddiqui[22], C. Soubiran[23], N. A. Walton[3], F. Arenou[2], U. Bastian[11], M. Cropper[24], R. Drimmel[25], D. Katz[2], M. G. Lattanzi[25], J. Bakker[15], C. Cacciari[26], J. Castañeda[5], L. Chaoul[18], N. Cheek[27], F. De Angeli[3], C. Fabricius[5], R. Guerra[15], B. Holl[12], E. Masana[5], R. Messineo[28], N. Mowlavi[12], K. Nienartowicz[29], P. Panuzzo[2], J. Portell[5], M. Riello[3], G. M. Seabroke[24], P. Tanga[17], F. Thévenin[17], G. Gracia-Abril[30,11], G. Comoretto[22], M. Garcia-Reinaldos[15], D. Teyssier[22], M. Altmann[11,31], R. Andrae[10], M. Audard[12], I. Bellas-Velidis[32], K. Benson[24], J. Berthier[33], R. Blomme[34], P. Burgess[3], G. Busso[3], B. Carry[17,33], A. Cellino[25], G. Clementini[26], M. Clotet[5], O. Creevey[17], M. Davidson[35], J. De Ridder[36], L. Delchambre[37], A. Dell'Oro[21], C. Ducourant[23], J. Fernández-Hernández[38], M. Fouesneau[10], Y. Frémat[34], L. Galluccio[17], M. García-Torres[39], J. González-Núñez[27,40], J. J. González-Vidal[5], E. Gosset[37,20], L. P. Guy[29,41], J.-L. Halbwachs[42], N. C. Hambly[35], D. L. Harrison[3,43], J. Hernández[15], D. Hestroffer[33], S. T. Hodgkin[3], A. Hutton[44], G. Jasniewicz[45], A. Jean-Antoine-Piccolo[18], S. Jordan[11], A. J. Korn[46], A. Krone-Martins[47], A. C. Lanzafame[48,49], T. Lebzelter[50], W. Löffler[11], M. Manteiga[51,52], P. M. Marrese[53,54], J. M. Martín-Fleitas[44], A. Moitinho[47], A. Mora[44], K. Muinonen[55,56], J. Osinde[57], E. Pancino[21,54], T. Pauwels[34], J.-M. Petit[58], A. Recio-Blanco[17], P. J. Richards[59], L. Rimoldini[29], A. C. Robin[58], L. M. Sarro[60], C. Siopis[19], M. Smith[24], A. Sozzetti[25], M. Süveges[10], J. Torra[5], W. van Reeven[44], U. Abbas[25], A. Abreu Aramburu[61], S. Accart[62], C. Aerts[36,63], G. Altavilla[53,54,26], M. A. Álvarez[51], R. Alvarez[15], J. Alves[50], R. I. Anderson[64,12], A. H. Andrei[65,66,31], E. Anglada Varela[38], E. Antiche[5], T. Antoja[9,5], B. Arcay[51], T. L. Astraatmadja[10,67], N. Bach[44], S. G. Baker[24], L. Balaguer-Núñez[5], P. Balm[22], C. Barache[31], C. Barata[47], D. Barbato[68,25], F. Barblan[12], P. S. Barklem[46], D. Barrado[69], M. Barros[47], S. Bartholomé Muñoz[5], J.-L. Bassilana[62], U. Becciani[49], M. Bellazzini[26], A. Berihuete[70], S. Bertone[25,31,71], L. Bianchi[72], O. Bienaymé[42], S. Blanco-Cuaresma[12,23,73], T. Boch[42], C. Boeche[6], A. Bombrun[74], R. Borrachero[5], S. Bouquillon[31], G. Bourda[23], A. Bragaglia[26], L. Bramante[28], M. A. Breddels[75], N. Brouillet[23], T. Brüsemeister[11], E. Brugaletta[49], B. Bucciarelli[25], A. Burlacu[18], D. Busonero[25], A. G. Butkevich[14], R. Buzzi[25], E. Caffau[2], R. Cancelliere[76], G. Cannizzaro[77,63], R. Carballo[78], T. Carlucci[31], J. M. Carrasco[5], L. Casamiquela[5], M. Castellani[53], A. Castro-Ginard[5], P. Charlot[23], L. Chemin[79], A. Chiavassa[17], G. Cocozza[26], G. Costigan[8], S. Cowell[3], F. Crifo[2], M. Crosta[25], C. Crowley[74], J. Cuypers[†34], C. Dafonte[51], Y. Damerdji[37,80], A. Dapergolas[32], P. David[33], M. David[81], P. de Laverny[17], F. De Luise[82], R. De March[28], D. de Martino[83], R. de Souza[84], A. de Torres[74], J. Debosscher[36], E. del Pozo[44], M. Delbo[17], A. Delgado[3], H. E. Delgado[60], S. Diakite[58], C. Diener[3], E. Distefano[49], C. Dolding[24], P. Drazinos[85], J. Durán[57], B. Edvardsson[46], H. Enke[86], K. Eriksson[46], P. Esquej[87], G. Eynard Bontemps[18], C. Fabre[88], M. Fabrizio[53,54], S. Faigler[89], A. J. Falcão[90], M. Farràs Casas[5], L. Federici[26], G. Fedorets[55], P. Fernique[42], F. Figueras[5], F. Filippi[28], K. Findeisen[2], A. Fonti[28], E. Fraile[87], M. Fraser[3,91], B. Frézouls[18], M. Gai[25], S. Galleti[26], D. Garabato[51], F. García-Sedano[60], A. Garofalo[92,26], N. Garralda[5], A. Gavel[46], P. Gavras[2,32,85], J. Gerssen[86], R. Geyer[14], P. Giacobbe[25], G. Gilmore[3], S. Girona[93], G. Giuffrida[54,53], F. Glass[12], M. Gomes[47], M. Granvik[55,94], A. Gueguen[2,95], A. Guerrier[62], J. Guiraud[18], R. Gutiérrez-Sánchez[22], R. Haigron[2], D. Hatzidimitriou[85,32], M. Hauser[11,10], M. Haywood[2], U. Heiter[46], A. Helmi[75], J. Heu[2], T. Hilger[14], D. Hobbs[16], W. Hofmann[11], G. Holland[3], H. E. Huckle[24], A. Hypki[8,96], V. Icardi[28], K. Janßen[86], G. Jevardat de Fombelle[29], P. G. Jonker[77,63], Á. L. Juhász[97,98], F. Julbe[5], A. Karampelas[85,99], A. Kewley[3],

★ The full Table A.1 is only available at the CDS via anonymous ftp to cdsarc.u-strasbg.fr (130.79.128.5) or via http://cdsarc.u-strasbg.fr/viz-bin/qcat?J/A+A/616/A10

★★ Corresponding author: C. Babusiaux, e-mail: carine.babusiaux@univ-grenoble-alpes.fr

J. Klar[86], A. Kochoska[100,101], R. Kohley[15], K. Kolenberg[73,102,36], M. Kontizas[85], E. Kontizas[32], S. E. Koposov[3,103], G. Kordopatis[17], Z. Kostrzewa-Rutkowska[77,63], P. Koubsky[104], S. Lambert[31], A. F. Lanza[49], Y. Lasne[62], J.-B. Lavigne[62], Y. Le Fustec[105], C. Le Poncin-Lafitte[31], Y. Lebreton[2,106], S. Leccia[83], N. Leclerc[2], I. Lecoeur-Taibi[29], H. Lenhardt[11], F. Leroux[62], S. Liao[25,107,108], E. Licata[72], H. E. P. Lindstrøm[109,110], T. A. Lister[111], E. Livanou[85], A. Lobel[34], M. López[69], S. Managau[62], R. G. Mann[35], G. Mantelet[11], O. Marchal[2], J. M. Marchant[112], M. Marconi[83], S. Marinoni[53,54], G. Marschalkó[97,113], D. J. Marshall[114], M. Martino[28], G. Marton[97], N. Mary[62], D. Massari[75], G. Matijevič[86], T. Mazeh[89], P. J. McMillan[16], S. Messina[49], D. Michalik[16], N. R. Millar[3], D. Molina[5], R. Molinaro[83], L. Molnár[97], P. Montegriffo[26], R. Mor[5], R. Morbidelli[25], T. Morel[37], D. Morris[35], A. F. Mulone[28], T. Muraveva[26], I. Musella[83], G. Nelemans[63,36], L. Nicastro[26], L. Noval[62], W. O'Mullane[15,41], C. Ordénovic[17], D. Ordóñez-Blanco [29], P. Osborne[3], C. Pagani[4], I. Pagano[49], F. Pailler[18], H. Palacin[62], L. Palaversa[3,12], A. Panahi[89], M. Pawlak[115,116], A. M. Piersimoni[82], F.-X. Pineau[42], E. Plachy[97], G. Plum[2], E. Poggio[68,25], E. Poujoulet[117], A. Prša[101], L. Pulone[53], E. Racero[27], S. Ragaini[26], N. Rambaux[33], M. Ramos-Lerate[118], S. Regibo[36], C. Reylé[58], F. Riclet[18], V. Ripepi[83], A. Riva[25], A. Rivard[62], G. Rixon[3], T. Roegiers[119], M. Roelens[12], M. Romero-Gómez[5], N. Rowell[35], F. Royer[2], L. Ruiz-Dern[2], G. Sadowski[19], T. Sagristà Sellés[11], J. Sahlmann[15,120], J. Salgado[121], E. Salguero[38], N. Sanna[21], T. Santana-Ros[96], M. Sarasso[25], H. Savietto[122], M. Schultheis[17], E. Sciacca[49], M. Segol[123], J. C. Segovia[27], D. Ségransan[12], I-C. Shih[2], L. Siltala[55,124], A. F. Silva[47], R. L. Smart[25], K. W. Smith[10], E. Solano[69,125], F. Solitro[28], R. Sordo[6], S. Soria Nieto[5], J. Souchay[31], A. Spagna[25], F. Spoto[17,33], U. Stampa[11], I. A. Steele[112], H. Steidelmüller[14], C. A. Stephenson[22], H. Stoev[126], F. F. Suess[3], J. Surdej[37], L. Szabados[97], E. Szegedi-Elek[97], D. Tapiador[127,128], F. Taris[31], G. Tauran[62], M. B. Taylor[129], R. Teixeira[84], D. Terrett[59], P. Teyssandier[31], W. Thuillot[33], A. Titarenko[17], F. Torra Clotet[130], C. Turon[2], A. Ulla[131], E. Utrilla[44], S. Uzzi[28], M. Vaillant[62], G. Valentini[82], V. Valette[18], A. van Elteren[8], E. Van Hemelryck[34], M. Vaschetto[28], A. Vecchiato[25], J. Veljanoski[75], Y. Viala[2], D. Vicente[93], S. Vogt[119], C. von Essen[132], H. Voss[5], V. Votruba[104], S. Voutsinas[35], G. Walmsley[18], M. Weiler[5], O. Wertz[133], T. Wevers[3,63], Ł. Wyrzykowski[3,115], A. Yoldas[3], M. Žerjal[100,134], H. Ziaeepour[58], J. Zorec[135], S. Zschocke[14], S. Zucker[136], C. Zurbach[45], and T. Zwitter[100]

(Affiliations can be found after the references)

Received 16 February 2018 / Accepted 16 April 2018

ABSTRACT

Context. *Gaia* Data Release 2 provides high-precision astrometry and three-band photometry for about 1.3 billion sources over the full sky. The precision, accuracy, and homogeneity of both astrometry and photometry are unprecedented.

Aims. We highlight the power of the *Gaia* DR2 in studying many fine structures of the Hertzsprung-Russell diagram (HRD). *Gaia* allows us to present many different HRDs, depending in particular on stellar population selections. We do not aim here for completeness in terms of types of stars or stellar evolutionary aspects. Instead, we have chosen several illustrative examples.

Methods. We describe some of the selections that can be made in *Gaia* DR2 to highlight the main structures of the *Gaia* HRDs. We select both field and cluster (open and globular) stars, compare the observations with previous classifications and with stellar evolutionary tracks, and we present variations of the *Gaia* HRD with age, metallicity, and kinematics. Late stages of stellar evolution such as hot subdwarfs, post-AGB stars, planetary nebulae, and white dwarfs are also analysed, as well as low-mass brown dwarf objects.

Results. The *Gaia* HRDs are unprecedented in both precision and coverage of the various Milky Way stellar populations and stellar evolutionary phases. Many fine structures of the HRDs are presented. The clear split of the white dwarf sequence into hydrogen and helium white dwarfs is presented for the first time in an HRD. The relation between kinematics and the HRD is nicely illustrated. Two different populations in a classical kinematic selection of the halo are unambiguously identified in the HRD. Membership and mean parameters for a selected list of open clusters are provided. They allow drawing very detailed cluster sequences, highlighting fine structures, and providing extremely precise empirical isochrones that will lead to more insight in stellar physics.

Conclusions. *Gaia* DR2 demonstrates the potential of combining precise astrometry and photometry for large samples for studies in stellar evolution and stellar population and opens an entire new area for HRD-based studies.

Key words. parallaxes – Hertzsprung-Russell and C-M diagrams – solar neighborhood – stars: evolution

1. Introduction

The Hertzsprung-Russell diagram (HRD) is one of the most important tools in stellar studies. It illustrates empirically the relationship between stellar spectral type (or temperature or colour index) and luminosity (or absolute magnitude). The position of a star in the HRD is mainly given by its initial mass, chemical composition, and age, but effects such as rotation, stellar wind, magnetic field, detailed chemical abundance, overshooting, and non-local thermal equilibrium also play a role. Therefore, the detailed HRD features are important to constrain stellar structure and evolutionary studies as well as stellar atmosphere modelling. Up to now, a proper understanding of the physical process in the stellar interior and the exact contribution of each of the effects mentioned are missing because we lack large precise and homogeneous samples that cover the full

HRD. Moreover, a precise HRD provides a great framework for exploring stellar populations and stellar systems.

Up to now, the most complete solar neighbourhood empirical HRD could be obtained by combining the HIPPARCOS data (Perryman et al. 1995) with nearby stellar catalogues to provide the faint end (e.g. Gliese & Jahreiß 1991; Henry & Jao 2015). Clusters provide empirical HRDs for a range of ages and metal contents and are therefore widely used in stellar evolution studies. To be conclusive, they need homogeneous photometry for inter-comparisons and astrometry for good memberships.

With its global census of the whole sky, homogeneous astrometry, and photometry of unprecedented accuracy, *Gaia* DR2 is setting a new major step in stellar, galactic, and extragalactic studies. It provides position, trigonometric parallax, and proper motion as well as three broad-band magnitudes (G, $G_{\rm BP}$, and $G_{\rm RP}$) for more than a billion objects brighter than $G \sim 20$, plus radial velocity for sources brighter than $G_{\rm RVS} \sim 12$ mag and photometry for variable stars (Gaia Collaboration 2018a). The amount, exquisite quality, and homogeneity of the data allows reaching a level of detail in the HRDs that has never been reached before. The number of open clusters with accurate parallax information is unprecedented, and new open clusters or associations will be discovered. *Gaia* DR2 provides absolute parallax for faint red dwarfs and the faintest white dwarfs for the first time.

This paper is one of the papers accompanying the *Gaia* DR2 release. The following papers describe the data used here: Gaia Collaboration (2018a) for an overview, Lindegren et al. (2018) for the astrometry, Evans et al. (2018) for the photometry, and Arenou et al. (2018) for the global validation. Someone interested in this HRD paper may also be interested in the variability in the HRD described in Gaia Collaboration (2018b), in the first attempt to derive an HRD using temperatures and luminosities from the *Gaia* DR2 data of Andrae et al. (2018), in the kinematics of the globular clusters discussed in Gaia Collaboration (2018c), and in the field kinematics presented in Gaia Collaboration (2018d).

In this paper, Sect. 2 presents a global description of how we built the *Gaia* HRDs of both field and cluster stars, the filters that we applied, and the handling of the extinction. In Sect. 3 we present our selection of cluster data; the handling of the globular clusters is detailed in Gaia Collaboration (2018c) and the handling of the open clusters is detailed in Appendix A. Section 4 discusses the main structures of the *Gaia* DR2 HRD. The level of the details of the white dwarf sequence is so new that it leads to a more intense discussion, which we present in a separate Sect. 5. In Sect. 6 we compare clusters with a set of isochrones. In Sect. 7 we study the variation of the *Gaia* HRDs with kinematics. We finally conclude in Sect. 8.

2. Building the *Gaia* HRDs

This paper presents the power of the *Gaia* DR2 astrometry and photometry in studying fine structures of the HRD. For this, we selected the most precise data, without trying to reach completeness. In practice, this means selecting the most precise parallax and photometry, but also handling the extinction rigorously. This can no longer be neglected with the depth of the *Gaia* precise data in this release.

2.1. Data filtering

The *Gaia* DR2 is unprecedented in both the quality and the quantity of its astrometric and photometric data. Still, this is an intermediate data release without a full implementation of the complexity of the processing for an optimal usage of the data. A detailed description of the astrometric and photometric features is given in Lindegren et al. (2018) and Evans et al. (2018), respectively, and Arenou et al. (2018) provides a global validation of them. Here we highlight the features that are important to be taken into account in building *Gaia* DR2 HRDs and present the filters we applied in this paper.

Concerning the astrometric content (Lindegren et al. 2018), the median uncertainty for the bright source ($G < 14$ mag) parallax is 0.03 mas. The systematics are lower than 0.1 mas, and the parallax zeropoint error is about 0.03 mas. Significant correlations at small spatial scale between the astrometric parameters are also observed. Concerning the photometric content (Evans et al. 2018), the precision at $G = 12$ is around 1 mmag in the three passbands, with systematics at the level of 10 mmag.

Lindegren et al. (2018) described that a five-parameter solution is accepted only if at least six visibility periods are used (e.g. the number of groups of observations separated from other groups by a gap of at least four days, the parameter is named `visibility_periods_used` in the *Gaia* archive). The observations need to be well spread out in time to provide reliable five-parameter solutions. Here we applied a stronger filter on this parameter: `visibility_periods_used>8`. This removes strong outliers, in particular at the faint end of the local HRD (Arenou et al. 2018). It also leads to more incompleteness, but this is not an issue for this paper.

The astrometric excess noise is the extra noise that must be postulated to explain the scatter of residuals in the astrometric solution. When it is high, it either means that the astrometric solution has failed and/or that the studied object is in a multiple system for which the single-star solution is not reliable. Without filtering on the astrometric excess noise, artefacts are present in particular between the white dwarf and the main sequence in the *Gaia* HRDs. Some of those stars are genuine binaries, but the majority are artefacts (Arenou et al. 2018). To still see the imprint of genuine binaries on the HRD while removing most of the artefacts, we adopted the filter proposed in Appendix C of Lindegren et al. (2018): $\sqrt{\chi^2/(\nu'-5)} < 1.2\max(1, \exp(-0.2(G-19.5))$ with χ^2 and ν' given as `astrometric_chi2_al` and `astrometric_n_good_obs_al`, respectively, in the *Gaia* archive. A similar clean-up of the HRD is obtained by the `astrometric_excess_noise<1` criterion, but this is less optimised for the bright stars because of the degrees of freedom (DOF) issue (Lindegren et al. 2018, Appendix A).

We built the *Gaia* HRDs by simply estimating the absolute *Gaia* magnitude in the G band for individual stars using $M_G = G + 5 + 5\log_{10}(\varpi/1000)$, with ϖ the parallax in milliarcseconds (plus the extinction, see next section). This is valid only when the relative precision on the parallax is lower than about 20% (Luri et al. 2018). We aim here to examine the fine structures in the HRD revealed by *Gaia* and therefore adopt a 10% relative precision criterion, which corresponds to an uncertainty on M_G smaller than 0.22 mag: `parallax_over_error>10`.

Similarly, we apply filters on the relative flux error on the G, $G_{\rm BP}$, and $G_{\rm RP}$ photometry: `phot_g_mean_flux_over_error>50` ($\sigma_G < 0.022$ mag), `phot_rp_mean_flux_over_error>20`, and `phot_bp_mean_flux_over_error>20` ($\sigma_{G_{\rm XP}} < 0.054$ mag). These criteria may remove variable stars, which are specifically studied in Gaia Collaboration (2018b).

The processing of the photometric data in DR2 has not treated blends in the windows of the blue and red photometers (BP and RP). As a consequence, the measured BP and RP fluxes may include the contribution of flux from nearby sources, the highest impact being in sky areas of high stellar density, such as

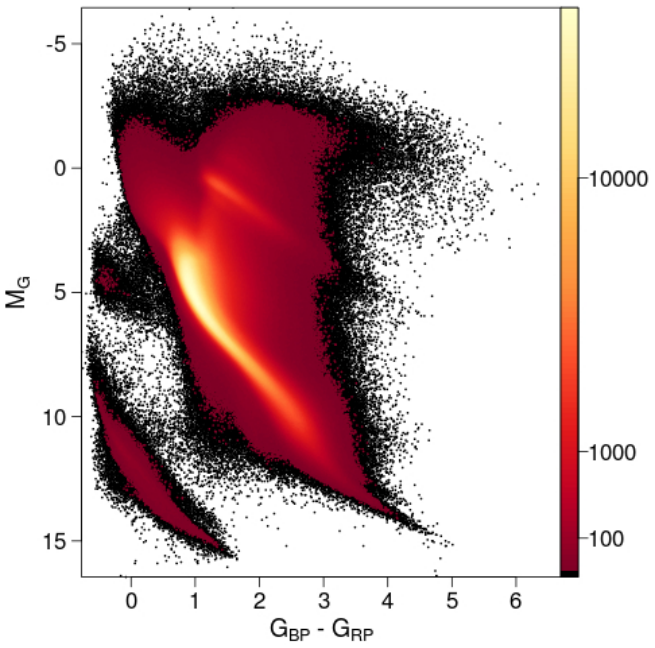

Fig. 1. Full *Gaia* colour-magnitude diagram of sources with the filters described in Sect. 2.1 applied (65 921 112 stars). The colour scale represents the square root of the relative density of stars.

the inner regions of globular clusters, the Magellanic Clouds, or the Galactic Bulge. During the validation process, misdeterminations of the local background have also been identified. In some cases, this background is due to nearby bright sources with long wings of the point spread function that have not been properly subtracted. In other cases, the background has a solar type spectrum, which indicates that the modelling of the background flux is not good enough. The faint sources are most strongly affected. For details, see Evans et al. (2018) and Arenou et al. (2018). Here, we have limited our analysis to the sources within the empirically defined locus of the $(I_{BP} + I_{RP})/I_G$ fluxes ratio as a function of $G_{BP} - G_{RP}$ colour: `phot_bp_rp_excess_factor`$> 1.0 + 0.015\ (G_{BP} - G_{RP})^2$ and `phot_bp_rp_excess_factor`$< 1.3 + 0.06\ (G_{BP} - G_{RP})^2$. The *Gaia* archive query combining all the filters presented here is provided in Appendix B.

2.2. Extinction

The dust that is present along the line of sight towards the stars leads to a dimming and reddening of their observed light. In the full colour – absolute magnitude diagram presented in Fig. 1, the effect of the extinction is particularly striking for the red clump. The de-reddened HRD using the extinction provided together with DR2 is presented in Andrae et al. (2018). To study the fine structures of the *Gaia* HRD for field stars, we selected here only low-extinction stars. High galactic latitude and close-by stars located within the local bubble (the reddening is almost negligible within ~60 pc of the Sun Lallement et al. 2003) are affected less from the extinction, and we did not apply further selection for them. To select low-extinction stars away from these simple cases, we followed Ruiz-Dern et al. (2018) and used the 3D extinction map of Capitanio et al. (2017)[1], which is particularly well adapted to finding holes in the interstellar medium and to select field stars with $E(B - V) < 0.015$.

[1] http://stilism.obspm.fr/

For globular clusters we used literature extinction values (Sect. 3.3), while for open clusters, they are derived together with the ages (Sect. 3.2). Detailed comparisons of these global cluster extinctions with those that can be derived from the extinctions provided by *Gaia* DR2 can be found in Arenou et al. (2018). To transform the global cluster extinction easily into the *Gaia* passbands while taking into account the extinction coefficients dependency on colour and extinction itself in these large passbands (e.g. Jordi et al. 2010), we used the same formulae as Danielski et al. (2018) to compute the extinction coefficients $k_X = A_X/A_0$:

$$k_X = c_1 + c_2(G_{BP} - G_{RP})_0 + c_3(G_{BP} - G_{RP})_0^2 + c_4(G_{BP} - G_{RP})_0^3 + c_5 A_0 + c_6 A_0^2 + c_7(G_{BP} - G_{RP})_0 A_0. \quad (1)$$

As in Danielski et al. (2018), this formula was fitted on a grid of extinctions convolving the latest *Gaia* passbands presented in Evans et al. (2018) with Kurucz spectra (Castelli & Kurucz 2003) and the Fitzpatrick & Massa (2007) extinction law for 3500 K $< T_{\rm eff} <$10 000 K by steps of 250 K, $0.01 < A_0 < 5$ mag by steps of 0.01 mag and two surfaces gravities: $\log g = 2.5$ and 4. The resulting coefficients are provided in Table 1. We assume in the following $A_0 = 3.1\,E(B - V)$.

Some clusters show high differential extinction across their field, which broadens their colour-magnitude diagrams. These clusters have been discarded from this analysis.

3. Cluster data

Star clusters can provide observational isochrones for a range of ages and chemical compositions. Most suitable are clusters with low and uniform reddening values and whose magnitude range is wide, which would limit our sample to the nearest clusters. Such a sample would, however, present a rather limited range in age and chemical composition.

3.1. Membership and astrometric solutions

Two types of astrometric solutions were applied. The first type is applicable to nearby clusters. For the second *Gaia* data release, the nearby "limit" was set at 250 pc. Within this limit, the parallax and proper motion data for the individual cluster members are sufficiently accurate to reflect the effects of projection along the line of sight, thus enabling the 3D reconstruction of the cluster. This is further described in Appendix A.1.

For these nearby clusters, the size of the cluster relative to its distance will contribute a significant level of scatter to the HRD if parallaxes for individual cluster members are not taken into account. With a relative accuracy of about 1% in the parallax measurement, an error contribution of around 0.02 in the absolute magnitude is possible. For a large portion of the *Gaia* photometry, the uncertainties are about 5–10 times lower, making the parallax measurement still the main contributor to the uncertainty in the absolute magnitude. The range of differences in parallax between the cluster centre and an individual cluster member depends on the ratio of the cluster radius over the cluster distance. At a radius of 15 pc, the 1% level is found for a cluster at 1.5 kpc, or a parallax of 0.67 mas. In *Gaia* DR2, formal uncertainties on the parallaxes may reach levels of just lower than 10 μas, but the overall uncertainty from localised systematics is about 0.025 mas. If this value is considered the 1% uncertainty level, then a resolution of a cluster along the line of sight, using *Gaia* DR2, becomes possible for clusters within 400 pc, and realistic for clusters within about 250 pc.

Table 1. Parameters used to derive the *Gaia* extinction coefficients as a function of colour and extinction (Eq. (1)).

	c_1	c_2	c_3	c_4	c_5	c_6	c_7
k_G	0.9761	−0.1704	0.0086	0.0011	−0.0438	0.0013	0.0099
k_{BP}	1.1517	−0.0871	−0.0333	0.0173	−0.0230	0.0006	0.0043
k_{RP}	0.6104	−0.0170	−0.0026	−0.0017	−0.0078	0.00005	0.0006

For clusters at larger distances, the mean cluster proper motion and parallax are derived directly from the observed astrometric parameters for the individual cluster members. The details of this procedure are presented in Appendix A.2.

3.2. Selection of open clusters

Our sample of open clusters consists of the mostly well-defined and fairly rich clusters within 250 pc, and a selection of mainly rich clusters at larger distances, covering a wider range of ages, mostly up to 1.5 kpc, with a few additional clusters at larger distances where these might supply additional information at more extreme ages. For very young clusters, the definition of the cluster is not always clear, as the youngest systems are mostly found embedded in OB associations, producing large samples of similar proper motions and parallaxes. Very few clusters appear to survive to an "old age", but those that do are generally rich, allowing good membership determination. The final selection consists of 9 clusters within 250 pc, and 37 clusters up to 5.3 kpc. Of the latter group, only 23 were finally used for construction of the colour-magnitude diagram; these clusters are listed together with the 9 nearby clusters in Table 2. For the remaining 14 clusters, the colour-magnitude diagrams appeared to be too much affected by interstellar reddening variations. More details on the astrometric solutions are provided in Appendix A; the solutions are presented for the nearby clusters in Table A.3 and for the more distant clusters in Table A.4. Figure 2 shows the combined HRD of these clusters, coloured according to their ages as provided in Table 2. The main-sequence turn-off and red clump evolution with age is clearly visible. The age difference is also shown for lower mass stars, the youngest stars lie slightly above the main sequence of the others. The white dwarf sequence is also visible.

3.3. Selection of globular clusters

The details of selecting globular clusters are presented in Gaia Collaboration (2018c). A major issue for the globular cluster data is the uncertainties on the parallaxes that result from the systematics, which is in most cases about one order of magnitude larger than the standard uncertainties on the mean parallax determinations for the globular clusters. The implication of this is that the parallaxes as determined with the *Gaia* data cannot be used to derive the distance moduli needed to prepare the composite HRD for the globular clusters. Instead, we had to rely on distances as quoted in the literature, for which we used the tables (2010 edition) provided online by Harris (1996). The inevitable drawback is that these distances and reddening values have been obtained through isochrone fitting, and the application of these values to the *Gaia* data will provide only limited new information. The main advantage is the possibility of comparing the HRDs of all globular clusters within a single, accurate photometric system. The combined HRD for 14 globular clusters is shown in Fig. 3, the summary data for these clusters is presented in Table 3. The photometric data originate predominantly from the outskirts of the clusters, as in the cluster centres the crowding often affects the colour index determination. Figure 3 shows the blue horizontal branch populated with the metal-poor clusters and the move of the giant branch towards the blue with decreasing metallicity.

An interesting comparison can be made between the most metal-rich well-populated globular cluster of our sample, 47 Tuc (NGC 104), and one of the oldest open clusters, M67 (NGC 2682) (Fig. 4). This provides the closest comparison between the HRDs of an open and a globular cluster. Most open clusters are much younger, while most globular clusters are much less metal rich.

Table 2. Overview of reference values used in constructing the composite HRD for open clusters (Fig. 2).

Cluster	DM	log(age)	[Fe/H]	$E(B-V)$	Memb
Hyades	3.389	8.90	0.13	0.001	480
Coma Ber	4.669	8.81	0.00	0.000	127
Pleiades	5.667	8.04	−0.01	0.045	1059
IC 2391	5.908	7.70	−0.01	0.030	254
IC 2602	5.914	7.60	−0.02	0.031	391
α Per	6.214	7.85	0.14	0.090	598
Praesepe	6.350	8.85	0.16	0.027	771
NGC 2451A	6.433	7.78	−0.08	0.000	311
Blanco 1	6.876	8.06	0.03	0.010	361
NGC 6475	7.234	8.54	0.02	0.049	874
NGC 7092	7.390	8.54	0.00	0.010	248
NGC 6774	7.455	9.30	0.16	0.080	165
NGC 2232	7.575	7.70	0.11	0.031	241
NGC 2547	7.980	7.60	−0.14	0.040	404
NGC 2516	8.091	8.48	0.05	0.071	1727
Trumpler 10	8.223	7.78	−0.12	0.056	407
NGC 752	8.264	9.15	−0.03	0.040	259
NGC 6405	8.320	7.90	0.07	0.139	544
IC 4756	8.401	8.98	0.02	0.128	515
NGC 3532	8.430	8.60	0.00	0.022	1802
NGC 2422	8.436	8.11	0.09	0.090	572
NGC 1039	8.552	8.40	0.02	0.077	497
NGC 6281	8.638	8.48	0.06	0.130	534
NGC 6793	8.894	8.78		0.272	271
NGC 2548	9.451	8.74	0.08	0.020	374
NGC 6025	9.513	8.18		0.170	431
NGC 2682	9.726	9.54	0.03	0.037	1194
IC 4651	9.889	9.30	0.12	0.040	932
NGC 2323	10.010	8.30		0.105	372
NGC 2447	10.088	8.74	−0.05	0.034	681
NGC 2360	10.229	8.98	−0.03	0.090	848
NGC 188	11.490	9.74	0.11	0.085	956

Notes. Distance moduli (DM) as derived from the *Gaia* astrometry; ages and reddening values as derived from *Gaia* photometry (see Sect. 6), with distances fixed on astrometric determinations; metallicities from Netopil et al. (2016); Memb: the number of members with *Gaia* photometric data after application of the photometric filters.

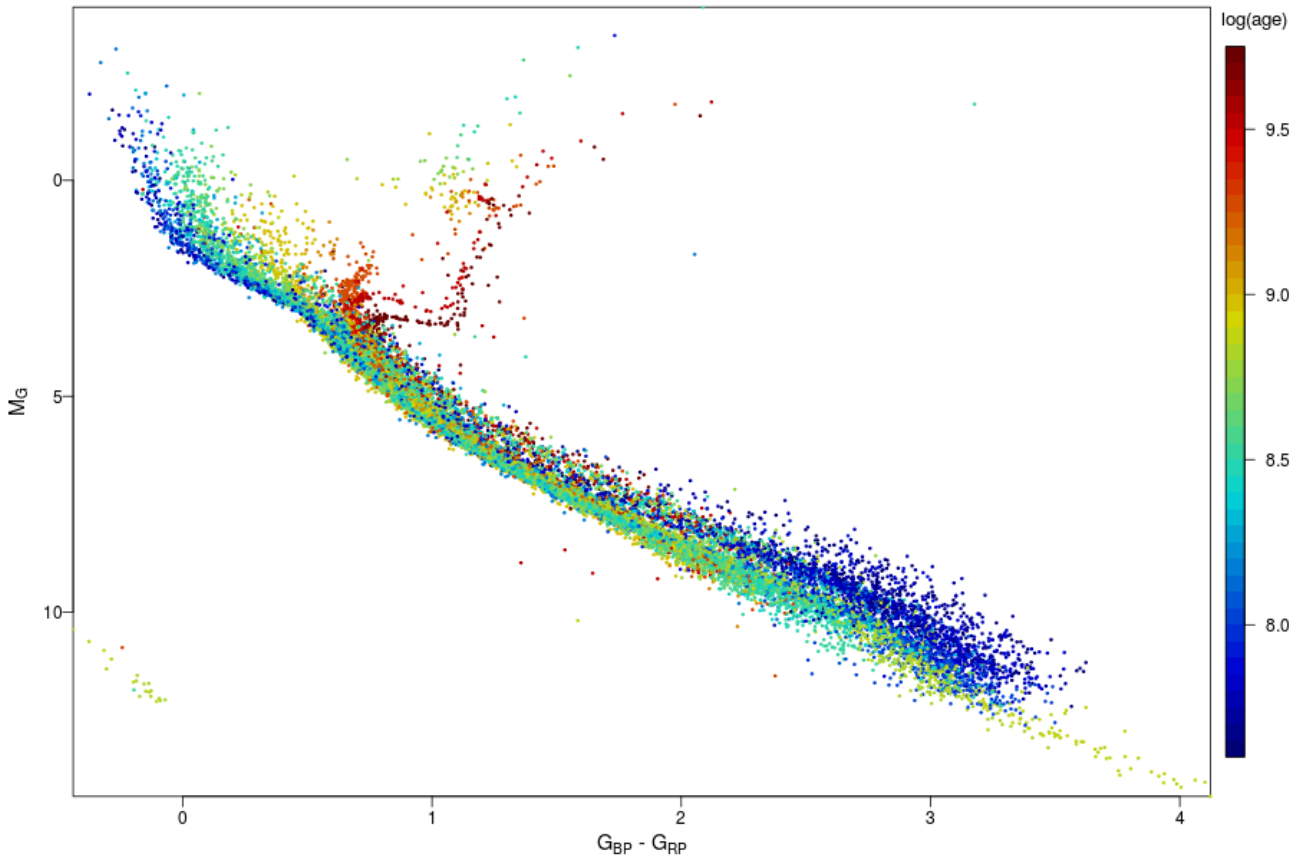

Fig. 2. Composite HRD for 32 open clusters, coloured according to log(age), using the extinction and distance moduli as determined from the *Gaia* data (Table 2).

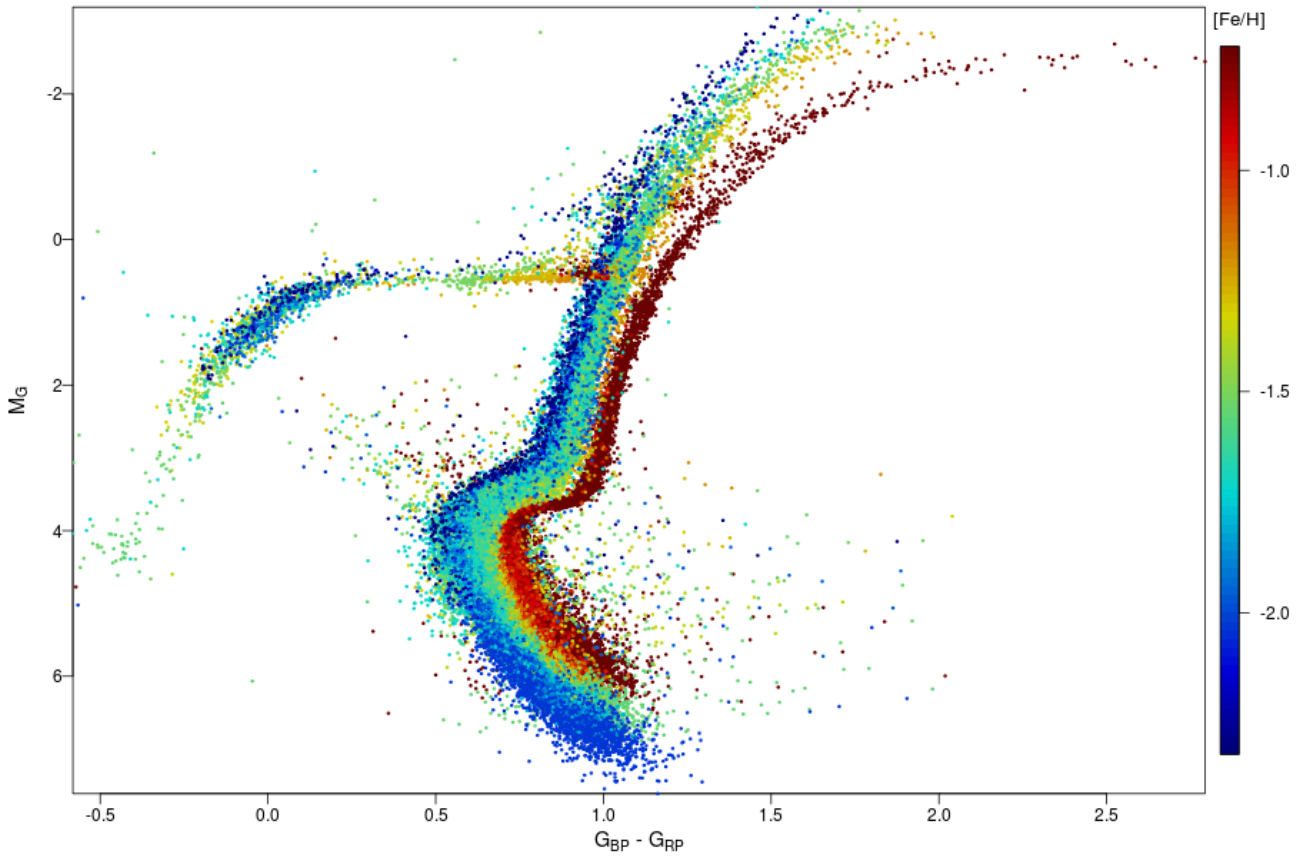

Fig. 3. Composite HRD for 14 globular clusters, coloured according to metallicity (Table 3).

Table 3. Reference data for 14 globular clusters used in the construction of the combined HRD (Fig. 3).

NGC	DM	Age (Gyr)	[Fe/H]	$E(B-V)$	Memb
104	13.266	12.75[a]	−0.72	0.04	21580
288	14.747	12.50[a]	−1.31	0.03	1953
362	14.672	11.50[a]	−1.26	0.05	1737
1851	15.414	13.30[c]	−1.18	0.02	744
5272	15.043	12.60[b]	−1.50	0.01	9086
5904	14.375	12.25[a]	−1.29	0.03	3476
6205	14.256	13.00[a]	−1.53	0.02	10311
6218	13.406	13.25[a]	−1.37	0.19	3127
6341	14.595	13.25[a]	−2.31	0.02	1432
6397	11.920	13.50[a]	−2.02	0.18	10055
6656	12.526	12.86[c]	−1.70	0.35	9542
6752	13.010	12.50[a]	−1.54	0.04	10779
6809	13.662	13.50[a]	−1.94	0.08	8073
7099	14.542	13.25[a]	−2.27	0.03	1016

Notes. Data on distance moduli (DM), [Fe/H] and $E(B–V)$ from Harris (1996), 2010 edition, [(a)] Dotter et al. (2010), [(b)] Denissenkov et al. (2017), [(c)] Powalka et al. (2017) for age estimates. Memb: cluster members with photometry after application of photometric filters.

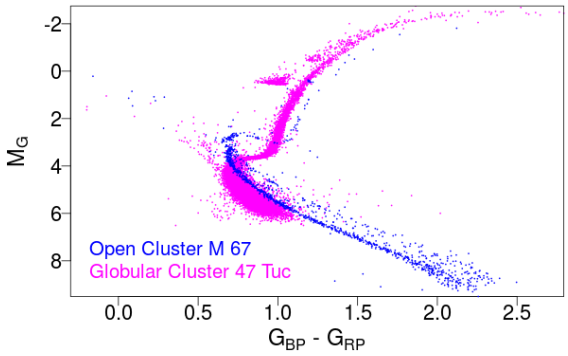

Fig. 4. Comparison between the HRDs of 47 Tuc (NGC 104, Age = 12.75 Gyr, [Fe/H] = −0.72), one of the most metal-rich globular clusters (magenta dots), and M 67 (NGC 2682, Age = 3.47 Gyr, [Fe/H] = 0.03), one of the oldest open clusters (blue dots).

4. Details of the *Gaia* HRDs

In the following, several field star HRDs are presented. Unless otherwise stated, the filters presented in Sect. 2.1, including the $E(B-V) < 0.015$ mag criteria, were applied. The HRDs use a red colour scale that represents the square root of the density of stars. The *Gaia* DR2 HRD of the low-extinction stars is represented in Fig. 5. The approximate equivalent temperature and luminosity to the $G_{BP} - G_{RP}$ colour and the absolute *Gaia* M_G magnitude provided in the figure were determined using the PARSEC isochrones (Marigo et al. 2017) for main-sequence stars.

Figure 6 shows the local *Gaia* HRDs using several cuts in parallax, still with the filters of Sect. 2.1, but without the need to apply the $E(B-V) < 0.015$ mag extinction criteria, as these sources mostly lie within the local bubble.

4.1. Main sequence

The main sequence is very thin, both in fields and in clusters. This is very clearly visible in Fig. 7, which shows the HRDs of

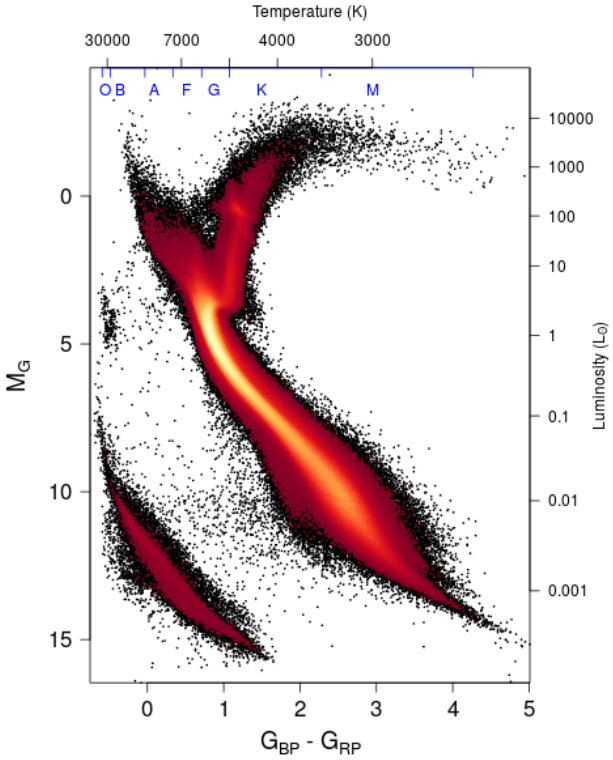

Fig. 5. *Gaia* HRD of sources with low extinction ($E(B–V) <$ 0.015 mag) satisfying the filters described in Sect. 2.1 (4 276 690 stars). The colour scale represents the square root of the density of stars. Approximate temperature and luminosity equivalents for main-sequence stars are provided at the top and right axis, respectively, to guide the eye.

the Hyades and Praesepe clusters (ages ∼700 Myr), which accurately overlap, as has previously been noticed in van Leeuwen (2009) and confirmed in Gaia Collaboration (2017). This figure shows the very narrow sequence described by the stars in both clusters, as well as the scattering of double stars up to 0.75 magnitudes above the main sequence. The remaining width of the main sequence is still largely explained as due to the uncertainties in the parallax of the individual stars, and the underlying main sequence is likely to be even narrower.

The binary sequence spread is visible throughout the main sequence (Figs. 5 and 6), and most clearly in open clusters (Fig. 7, see also Sect. 6). It is most preeminent for field stars below $M_G = 13$. Figure 8 shows the main-sequence fiducial of the local HRD shifted by 0.753 mag, which corresponds to two identical stars in an unresolved binary system observed with the same colour but twice the luminosity of the equivalent single star. See Hurley & Tout (1998), for instance, for a discussion of this strong sequence. Binaries with a main-sequence primary and a giant companion would lie much higher in the diagram, while binaries with a late-type main-sequence primary and a white dwarf companion lie between the white dwarf and the main sequence, as is shown in Fig. 5, for example.

The main sequence is thicker between $10 < M_G < 13$ (Figs. 2, 5 and 6). The youngest main-sequence stars lie on the upper part of the main sequence (in blue in Fig. 2). The subdwarfs, which are metal-poor stars associated with the halo, are visible in the lower part of the local HRD (in red in Fig. 2, see also Sect. 7).

The main-sequence turn-off variation with age is clearly illustrated in Fig. 2, and the variation with metallicity is shown

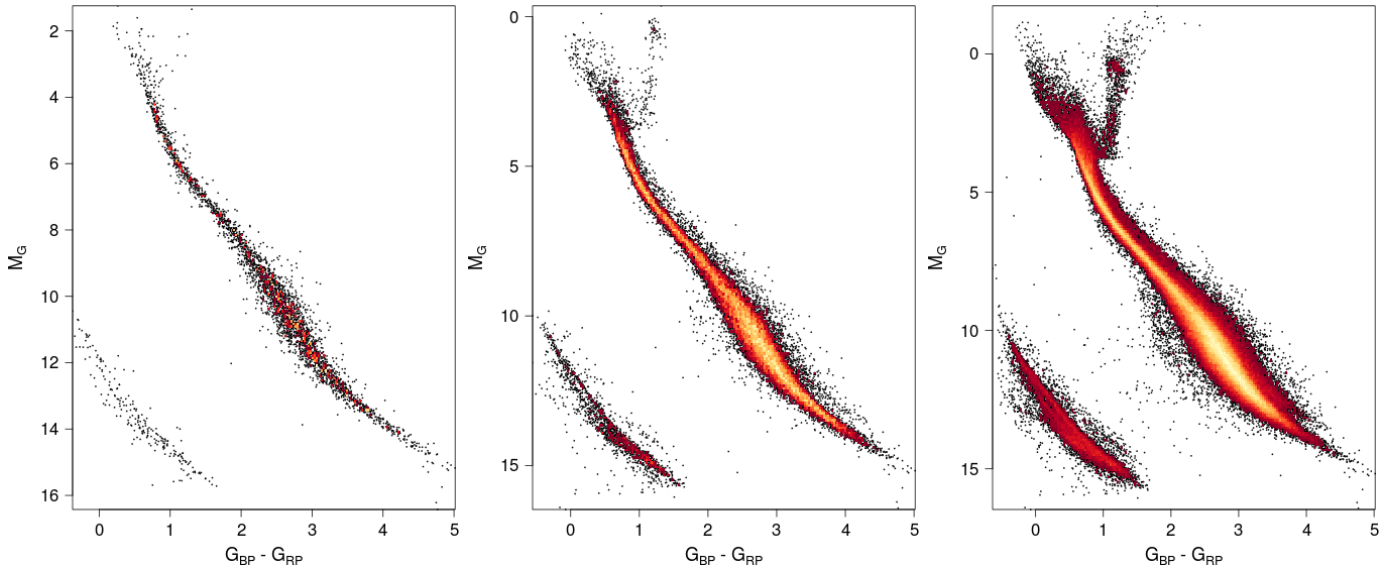

Fig. 6. Solar neighbourhood *Gaia* HRDs for *panel a*: $\varpi > 40$ mas (25 pc, 3724 stars), *panel b*: $\varpi > 20$ mas (50 pc, 29 683 stars), and *panel c*: $\varpi > 10$ mas (100 pc, 212 728 stars).

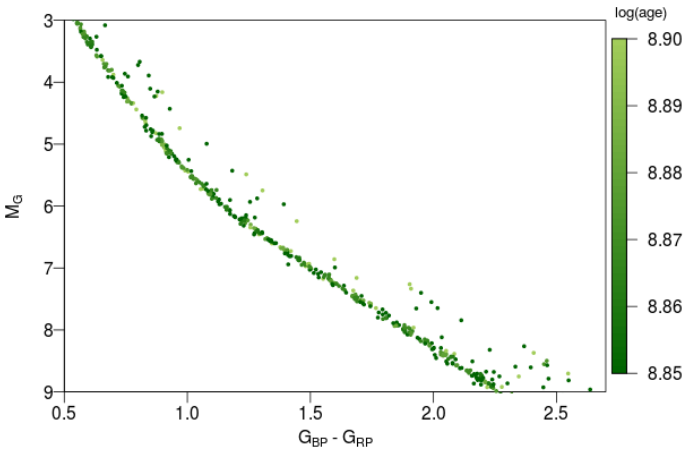

Fig. 7. Extract of the HRD for the Hyades and Praesepe clusters, showing the detailed agreement between the main sequences of the two clusters, the narrowness of the combined main sequence, and a scattering of double stars up to 0.75 mag above the main sequence.

in Fig. 3. Blue stragglers are also visible over the main-sequence turn-off (Fig. 4).

Between the main sequence and the subgiants lies a tail of stars around $M_G = 4$ and $G_{BP} - G_{RP} = 1.5$. These stars shows variability and may be associated with RS Canum Venaticorum variables, which are close binary stars (Gaia Collaboration 2018b).

4.2. Brown dwarfs

To study the location of the low-mass objects in the *Gaia* HRD, we used the *Gaia* ultracool dwarf sample (GUCDS) compiled by Smart et al. (2017). It includes 1886 brown dwarfs (BD) of L, T, and Y types, although a substantial fraction of them are too faint for *Gaia*. We note that the authors found 328 BDs in common with the *Gaia* DR1 catalogue (Gaia Collaboration 2016).

The crossmatch between the 2MASS catalogue (Skrutskie et al. 2006) and *Gaia* DR2 provided within the *Gaia* archive (Marrese et al. 2018) has been used to identify GUCDS entries. The resulting sample includes 601 BDs. Of these, 527 have

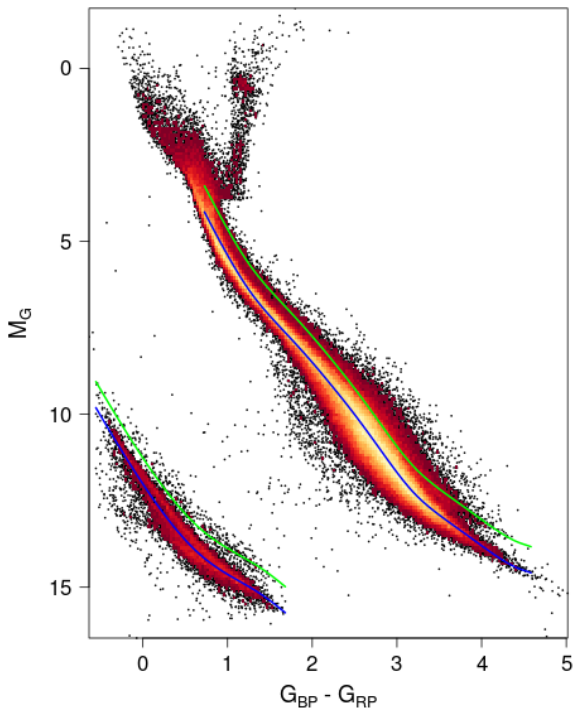

Fig. 8. Same as Fig. 6c, overlaid in blue with the median fiducial and in green with the same fiducial shifted by −0.753 mag, corresponding to an unresolved binary system of two identical stars.

five-parameter solutions (coordinates, proper motions, and parallax) and full photometry (G, G_{BP}, and G_{RP}). Most of these BDs have parallaxes higher than 4 mas (equivalent to 250 pc in distance) and relative parallax errors smaller than 25%. They also have astrometric excess noise larger than 1 mas and a high $(I_{BP} + I_{RP})/I_G$ flux ratio. They are faint red objects with very low flux in the BP wavelength range of their spectrum. Any background under-estimation causes the measured BP flux to increase to more than it should be, yielding high flux ratios, the highest ratios are derived for the faintest BDs. The filters presented in Sect. 2.1 therefore did not allow us to retain them.